Cement and Concrete Research 42 (2012) 291–305

Contents lists available at SciVerse ScienceDirect

Cement and Concrete Research

journal homepage: http://ees.elsevier.com/CEMCON/default.asp

Impact load-induced micro-structural damage and micro-structure associated mechanical response of concrete made with different surface roughness and porosity aggregates

Savaş Erdem *, Andrew Robert Dawson, Nicholas Howard Thom

School of Civil Engineering, Faculty of Engineering, University of Nottingham, University Park, Nottingham NG7 2RD, UK

ARTICLE INFO

Article history:
Received 12 April 2011
Accepted 29 September 2011

Keywords:
Micro-damage
Micro-structure (B)
Aggregate (D)
Concrete (E)
Mechanical properties (C)

ABSTRACT

The relationship between the nature of micro damage under impact loading and changes in mechanical behavior associated with different microstructures is studied for concretes made with two different coarse aggregates having significant differences mainly in roughness and porosity — sintered fly ash and uncrushed gravel. A range of techniques including X-ray diffraction, digital image analysis, mercury porosimetry, X-ray computed tomography, laser surface profilometry and scanning electron microscopy were used to characterize the aggregates and micro-structures. The concrete prepared with lightweight aggregates was stronger in compression than the gravel aggregate concrete due to enhanced hydration as a result of internal curing. In the lightweight concrete, it was deduced that an inhomogeneous micro-structure led to strain incompatibilities and consequent localized stress concentrations in the mix, leading to accelerated failure. The pore structure, compressibility, and surface texture of the aggregates are of paramount importance for the micro-cracking growth.

1. Introduction

Concrete is a non-homogeneous material generally regarded as a multiphase composite made of three phases at microscopic level: coarse aggregate, matrix and an interfacial transition zone (ITZ) between the aggregates and the matrix. Among the constituents, the ITZ is structurally inferior as it contains, on average, more pores and soluble calcium hydroxide, and fewer cement grains than does bulk paste farther away [1].

In the study of the ITZ, the key question that needs to be answered is to what extent the existence of the ITZ has any practical influences on the engineering properties of concrete or is it just a peculiarity of academic interest? [2]. The general consensus for many conventional concrete is that the breakdown of the ITZ (the weakest link) will reduce solidity of the concrete and facilitate penetration of deleterious species into the concrete [3,4]. More specifically, under externally exposed loads and environmental effects, the occurrence of tensile stress leads to the growth of micro-cracks in the ITZ both in size and number, and the penetration of the ITZ cracks into the surrounding matrix. The eventual joining of the micro-cracks yields large cracks and failure results [5].In conventional concrete, there is a "wall effect", in which the aggregates appear locally flat to the cement grains and disrupt their packing. In some lightweight aggregate concretes, this does not exist and a nearly continuous uniform microstructure of hydration products abuts and partially penetrates the lightweight aggregates [6]. This difference has a pronounced effect on crack initiation and propagation. Moreover, the lightweight aggregate-cement paste can be characterized by a mechanical interlocking in combination with a chemical interaction in the form of pozzolanic reaction [7] and lightweight aggregates can act as an internal water reservoir ("internal curing") when they are saturated (prewetted) and may increase the degree of hydration of cement [8]. As a result of these effects, the lightweight aggregate-cement paste bond strength is usually higher than the conventional aggregate-cement paste bond strength. Although the affected part of the mix is small, this can have a very significant influence on the concrete strength if the interface would otherwise be the weakest part of the microstructural system.

Lightweight aggregate is usually weaker than both conventional aggregate and cement mortar. On this basis one might expect the concrete to be weaker, too. If, however, the lightweight aggregate is stronger than the ITZ in conventional mix, then this expectation might not be met. For example, a recent study conducted by Kayali [9] showed that concrete produced with sintered fly ash lightweight aggregates was 20% stronger in compression than concrete made with conventional aggregates under the same mix design conditions although the lightweight aggregate was weaker than the ordinary aggregates. Unfortunately, the author did not conduct any quantitative microstructural work, and based on qualitative analysis, the author attributed the higher strength to the strong bonding characteristics

* Corresponding author. Tel.: +44 115 823 2424; fax: +44 115 951 3909.
E-mail address: evxse1@nottingham.ac.uk (S. Erdem).

0008-8846/$ – see front matter © 2011 Elsevier Ltd. All rights reserved.
doi:10.1016/j.cemconres.2011.09.015

that develop at the cement paste and the lightweight aggregate. In addition, it was observed that cracking did not initiate at the interfaces but rather was arrested by the interfacial zone. This means that the ITZ in conventional concrete could be weaker than the lightweight aggregate and, thus, the high strength of other materials is inconsequential if failure is primarily in the ITZ which is stronger for the mixes. Overall, it appears that there are conflicting arguments and continuing uncertainty about the significance of the ITZ with regard to the overall concrete behavior.

In practice, structural concrete can be subjected to a range of high loading rates stemming from dropped objects, vehicle collisions, missile impacts, explosion, etc. [10]. The behavior of concrete under impact loading is significantly different than that under static or seismic loads as concrete is a strain-rate sensitive material and its properties change with changes in the rate of loading [11,12]. Theoretically, the small cracks that lead to the non-linearity in the static case are pushed to propagate much more quickly under impact loading. Thus, cracks are prone to propagate across aggregates rather than around them, leading to an increase in strength and toughness, and a decrease in the non-linear portion of the stress–strain curve [13]. In the literature, a significant number of studies have been performed investigating the impact behavior of conventional and fiber-reinforced concrete at a macro level [14–16], however research conducted so far is still too limited to clarify the micro damage and micro failure mechanism of concrete subjected to high rates of loading. This leads to the objective of this study, which is to analyze the micro-damage characteristics of concrete that has experienced impact loading, so as to assess the influence of the characteristics (strength, shape, surface texture etc.) of coarse aggregate. A complementary objective is to make a comparison between the mechanical, load-deflection, responses of concrete and its microstructure as exemplified in mixes made with lightweight sintered fly ash aggregates and conventional aggregates.

2. Materials and methodology

2.1. Properties of materials used in concrete production

The fly ash aggregates (FAA) reported here (commercially known as Lytag), were manufactured by pelletising the fly ash at a temperature of around 1100 °C. The manufactured aggregates are rounded in shape and range in size from 14 mm down to 4 mm. The chemical composition obtained from X-ray fluorescence (XRF) of the FAA is shown in Table 1. Uncrushed gravel sourced from a local quarry with a nominal maximum size of 14 mm was used to produce a control (reference) mix. General purpose Portland-fly ash cement CEM II/B-V 32.5 R conforming to BS EN 197–1: 2000 [17] was used to produce all the concrete mixes. Local river sand complying with the requirements of BS EN 13139: 2002 [18] with a specific gravity of 2660 kg/m^3 constituted the fine aggregate in all mixes.

2.2. Production of concrete mixtures

In all mixes, the volume fractions of cement, coarse aggregates, sand and free water were the same. The only difference was the type of coarse aggregate used in the mixtures. The mix proportions are given in Table 2. The same size percentages were selected for the lightweight fly ash and normal weight aggregates to eliminate the effect of grading difference on concrete performance. The grading of the lightweight and conventional aggregates conformed to the requirements given in the relevant British European Standard is presented in Table 3. All concrete mixtures were batched using a mechanical pan mixer. In mixing, the dry ingredients (cement, sand and coarse aggregates) were always blended first, and then water was gradually added. In the case of lightweight concrete, the lightweight aggregates were first immersed in water for 24 h until all particles were fully saturated before the mixing, and subsequently air dried in the laboratory to obtain, approximately, a saturated surface dry condition. In this condition, the aggregates cannot absorb any more water. Depending on the relative osmotic and matric suctions developed by the curing cement paste and the pores within the lightweight aggregate pieces, some water might be drawn from the aggregate, but this (if occurs) cannot be quantified so the amount of absorbed water is not included in the calculation of mix water. Thereafter, the fresh concrete was filled into steel molds in two layers and then consolidated using a vibration table to release possible entrained air voids and covered with plastic sheets to prevent moisture loss from the concrete surface. The specimens were left in their molds for 1 day before de-molding and finally cured at 20 ± 2 °C in a water tank until the day of testing.

Table 1
Average chemical composition of fly ash aggregate (wt.% dry solid).

Component	SiO_2	Al_2O_3	Fe_2O_3	CaO	MgO	SO_3	Cl^-	Total sulfate	LOI[a]
Amount (%)	53.0	25.0	6.0	4.0	2.9	0.3	0.01	0.4	3.1

[a] Loss on ignition.

Table 2
Mix proportions for 1 m^3.

Material (kg/m^3)	Normal weight concrete	Lightweight concrete
Cement	330	330
Water	198	198
Sand	678	678
Gravel (coarse aggregate)	1115	0
Sintered fly ash (coarse aggregate)	0	566

2.3. Tests and analysis performed

2.3.1. Aggregate tests

Pore structure of the gravel and sintered fly ash aggregates were measured by mercury intrusion porosimetry (MIP) with a pressure applied up to 410 MPa, using a Quantachrome-PoreMaster Mercury porosimeter. The porosity and the critical pore diameter for each aggregate were calculated with the use of pore size distribution curves.

A digital image processing (DIP) technique was used to analyze the particle shape characteristics of the coarse aggregates. A Cambridge Instrument Quantimet 570™ DIP system connected to a CCD camera was used for image acquisition. After acquiring the images, a computer software program (Image Pro ™) was used for the quantification of aggregate shape characteristics. Surface roughness (Ra) of the aggregates was measured by stylus profilometry using a 2D Mitutoyo Surftest SV 662 profiler with a 5 μm stylus. Auto drive unit was used to measure the evaluation length at a speed of 0.2 mm/s. Ra is calculated as the total of the average height of the entire surface from the mean line within the sampling length. It should be noted that the equipment is normally used for the roughness measurement of metallic surfaces.

Table 3
Grading of the coarse aggregates.

Sieve size	% Passing	Lower limit % passing	Upper limit % passing
14	100	90	100
10	85.16	65	95
8	54.22	35	65
6.3	22.49	15	40
4	1.68	0	15

The physical properties of the aggregates were also determined based on standard procedure. The modulus of elasticity of the aggregates was calculated using the formula given by Muller-Rochholz [19], namely $E_a = 8.1\rho_a^2$ where ρ_a is density of aggregate. Given that the aggregate pieces are the largest available form of the FAA, it is impossible to determine modulus of elasticity from core (or similar) samples. Hence this formula has been used to determine the modulus of elasticity.

2.3.2. Hardened concrete tests

The density and compressive strengths were measured on 100 mm cubes in accordance with the relevant British European Standards. The dynamic modulus of elasticity of prismatic specimens was determined using a commercially available non-destructive ultrasonic device. The apparent porosity of tested specimens was also determined in accordance with Archimedes principle by measuring the weights of a saturated sample in water and in air, and the weight of the sample oven-dried at 100 ± 5 °C for 24 h. The flexural strength was tested on $100 \times 100 \times 500$ mm concrete beams with four-point flexural loading. This test was carried out using a closed-loop deflection controlled Zwick universal testing machine with a capacity of 200 kN at a constant deflection rate of 0.10 mm-min. All the tests were conducted at the age of 28 days.

2.3.3. Impact testing

The impact resistance of the concrete specimens was initially determined by an instrumented drop weight impact test arrangement that the authors developed in accordance with the suggestions of ACI Committee 544 [20]. The impact was achieved by dropping a 5 kg cylindrical steel mass with a hemispherical head from a height of 1 m onto a 100 mm cube under the guidance of a PVC tube (Fig. 1). The specimen was placed on a steel base plate that rests upon the concrete laboratory floor. There was a rubber sheet with a thickness of 3 mm that was also placed between the specimen and the base plate to prevent stress concentrations. A steel plate, 10 mm thick, was then positioned on the top of the concrete specimen to help generate uniform load distribution. A 25 mm diameter contact plate made of copper-coated mild steel was placed beneath the top plate to prevent its bending. A small pulley and nylon rope was used to hoist the mass to the required height and allow it to free fall when released. The impact resistance of the specimens was determined in terms of the number of blows required either to produce the first visible crack or to cause complete failure of the specimens.

2.3.3.1. Micro-structural damage evaluation. The loss of the dynamic modulus of elasticity, micro-crack concentrations at the ITZ and air void content/distribution before and after the impact testing in the concrete specimens were available as evaluation indexes for impact damage. The crack density (1/μm), equal to the micro-crack length per area unit, was calculated from the SEM images by dividing the total length of the cracks (μm) to the total examined surface area (μm^2). In order to investigate the void characteristics of the mixtures, sequences of 2D images were captured through the height of the 100 mm cube specimens with a slice thickness of 1 mm using the non-destructive X-ray CT system. The captured images from the X-ray CT system were then analyzed and converted to 3D images using an image analysis software package (Image J). In addition, a scalar variable ξ, suggested by Ying [21], was used to quantify the levels of damage in the specimens as follows: $\xi = 1 - (\bar{A}/A)$ where A is the initial area of the undamaged section and $\bar{A}$ is the effective cross sectional area in the current damaged state, which was calculated by subtracting the areas of air voids from the total cross sectional area.

2.3.3.2. Characterization of fracture surfaces. The quantitative analysis of the fracture surfaces after impact was made using a three-dimensional (3D) non-contact profilometer with a laser scanner, Talysurf CLI 1000 (Taylor Hobson). The surface inspection was carried out on one of the cracked halves of the specimen. The length of the measurement profiles

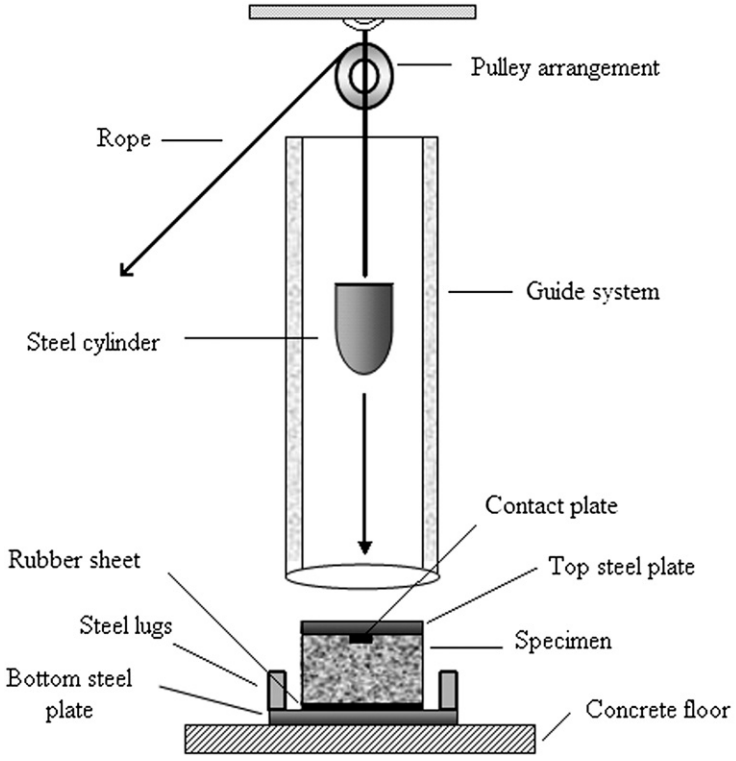

Fig. 1. Schematic diagram of the impact test set up.

was kept constant for all specimens so that the results are comparable. Finally, micro roughness value was calculated for each mix. A mean value of three measurements was used as a response value for each experiment. For a rough measure of fracture energy based on surface macro-crack, the formula suggested by Guo et al. [22] was adopted as follows: $Ws/Gf = a^{*}(\delta/a)^{1-D1\text{-}d}$ where Ws is the total energy dissipated at the surface of the crack; G_f is the fracture energy at the scale of observation δ (δ is equal to 5 mm — the maximum diameter of sand in concrete); a is the Euclidean length, which is equal to the height of the cross-section and $D_{1\text{-}d}$ is the mean value of the fractal dimension of surface cracks on the fractured specimen. The profiles of the crack maps of the specimens were obtained using the same image software that was used to calculate the fractal dimension.

2.3.4. SEM observation of concretes

The microstructure and morphology of the mixtures were observed on fractured surfaces using with secondary electron mode of the SEM. Fractured small samples were mounted on the SEM stubs and left under high vacuum, and then coated with carbon before capturing an image. The specimens were kept in a vacuum dessicator until used to minimize the surface carbonation due to the exposure of the samples to the CO_2 in the atmosphere. The microstructural features investigated in this study were porosity and unhydrated (UH) cement grain content. The quantification of the porosity in the ITZ has been performed by means of the technique developed by Scriven-er and Pratt [23]. The BSE images were captured at 540× magnification. The porosity profile and UH grain content for ITZ were analyzed up to 50 μm from the aggregate surface. The profile for the bulk paste was also determined using a similar technique, but the analysis was carried out at least 50 μm away from the nearest aggregate surface. Then, the ITZ and the bulk paste images were analyzed using Scandium image software. The ITZ thickness has been regarded as the distance from the aggregate surface where the porosity curves approach to the observed porosity of the bulk paste. Twenty fields were investigated for each sample.

2.3.5. Ca/Si ratio in the ITZ

X-ray line analysis was performed in the region of the aggregate-cement paste interfaces of the specimens to detect the presence of various elements. Ca/Si ratios were calculated for each element and plotted against the distance from the interfaces. The analysis was carried out at distances of 0–50 μm away from the surface of aggregate. It has been reported that the Ca/Si ratio for C–S–H is in the range 0.8 to 2.5; CH is above 10 and for monosulfate (AFm) is above 4 [24]. An example of the analysis is given in Fig. 2.

2.3.6. Thermogravimetric (TGA) analysis

The quantity of portlandite (CH) in mortar was determined by TGA. Analysis were conducted at heating rate of 3° per minute up to 220 °C and 10 °C per minute up to 600 °C in a nitrogen atmosphere. The weight loss-temperature (TGA) combined with derivative weight loss-temperature (DTG) profiles was recorded.

3. Results and discussions

3.1. Results of aggregate tests

The physical properties of the natural and sintered ash aggregates are given in Table 4. Comparison between the properties of FAA and those of gravel aggregates indicates that FAA is more porous, less dense and weaker than the gravel aggregate. The mineralogical analysis results of FAA by the XRD technique are shown in Fig. 3. This shows that the FAA contains, essentially, the crystalline phases of quartz, mullite and crystobolite together with smaller amounts of the crystalline phases of iron. However, some diffraction peaks, particularly at higher angles, could not be distinguished.

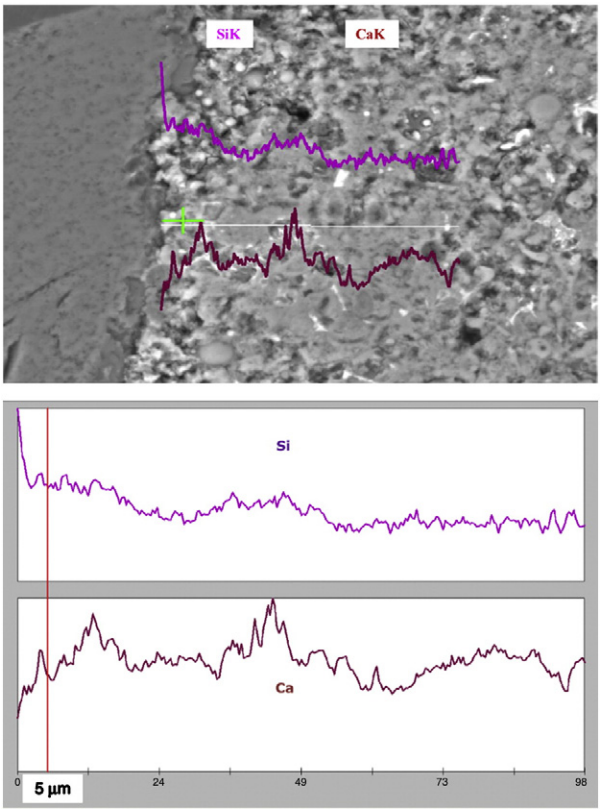

Fig. 2. Energy dispersive spectroscopy analysis in the ITZ.

The pore size distribution of the FAA and gravel aggregates is shown in Fig. 4. The pressures were converted into values of equivalent pore widths. The mercury intrusion porosities of the FAA and gravel aggregates are 52.7% and 1.62%, respectively. The higher porosities of FAA aggregates can be attributed to incomplete densification during the sintering process at high temperatures. The pores in the aggregates mainly distributed between 100 and 1 μm, and the threshold diameters – point at which there is a large change in slope – were about 0.6 μm.

Fig. 5 shows typical surface profiles of the gravel and FAA, and calculated results of surface roughness (Ra) are also given in this figure. In addition, the geometrical parameters of the FAA and gravel aggregates are also shown in Table 5. As expected, the FAA aggregate was more rounded, much rougher, less angular, and had a larger surface area than the gravel.

3.2. Engineering properties of concrete accompanied by the microstructure

The engineering properties of the conventional and fly ash lightweight concrete are tabulated in Table 6. Surprisingly enough, the results demonstrate that the concrete with FAA is stronger in compression than the concrete made with gravel aggregates, which contradicts the results of previous studies [25–27]. However, Hijazin and Lopez [28] and Bentz

Table 4
The physical and mechanical properties of aggregates used.

Characteristics	Gravel	Sintered fly ash
Specific gravity (Mg/m^3)	2.65	1.35
Dry rodded bulk density (kg/m^3)	1520	710
Crushing value (%)	16.7	34.6
Impact value (%)	12	24
Voids (%) rodded	42.60	47.40
The modulus of elasticity (GPa)	56.9	14.8

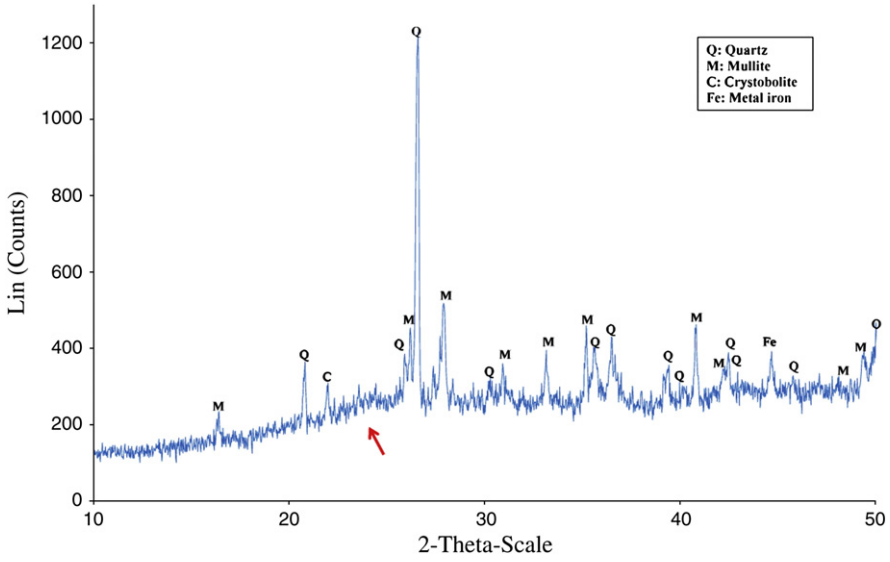

Fig. 3. XRD pattern of the sintered fly ash aggregate.

[29] showed that the mixtures with pre-wetted lightweight aggregates reached a higher compressive strength. The higher strength was attributed to the fact that a higher degree of hydration can overcome the reduction in strength caused by the use of a lower intrinsic strength lightweight aggregate.

The relatively higher compressive strength of the lightweight concrete could be attributed to combined effects of the localized high cement content in the vicinity of the pre-wetted aggregate and to the internal curing effect within the concrete. As wet lightweight fly ash aggregate was mixed with cement and sand before water addition, the lightweight aggregates were coated in cement, which affects local cement content around the aggregates after mixing. In parallel, internal curing water from the lightweight aggregate could gradually be released into the matrix with the progress of cement hydration process and most likely, encourage pozzolanic reaction with pulverized fly ash (PFA) from the cement, and thus influence the kinetics of the hydration process and further hydrate the paste. Furthermore, the absorbed water can also increase the pozzolanic reaction of Ca^{+2} with silica ions in the FAA as the XRD pattern indicates that the FAA has amorphous nature and pozzolanic characteristic (see Fig. 3 — the hump shown by a red arrow). The measurement of unhydrated cement grains in the ITZ could provide good support to the hypothesis of a locally higher degree of hydration within the lightweight concrete. Fig. 6 shows the curve of percentage of unhydrated cement (UH) versus distance from the aggregate interface. The analysis reveals that there was a gradual increase in the percentage of UH in both specimens with distance from the aggregate but the level of UH for gravel concrete was clearly higher than that of the lightweight concrete. More concentrated UH content in the case of gravel specimen signifies that less hydration has taken place and, hence, the presumption of a lower mechanical strength.

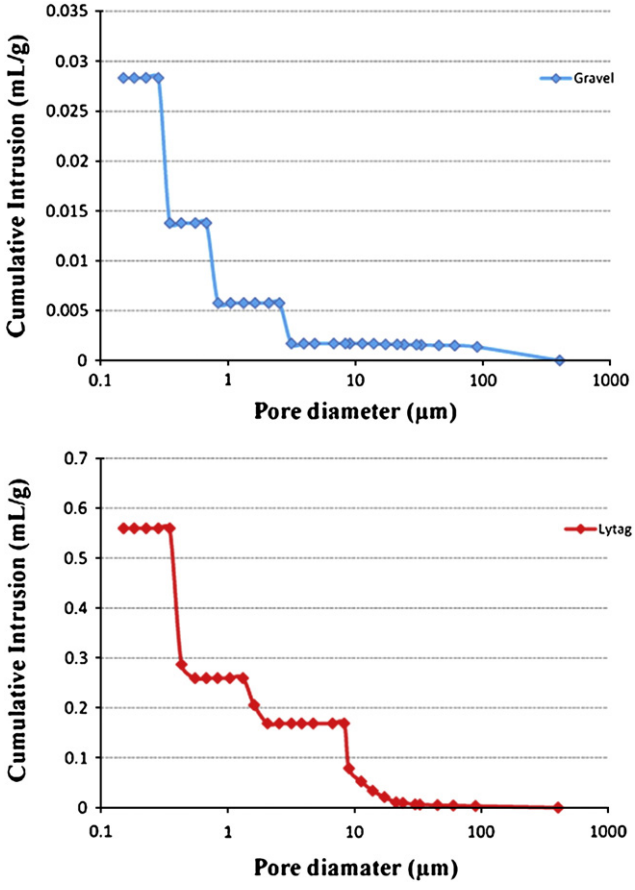

Fig. 4. Pore size distribution curves of gravel and fly ash aggregates.

Another way of supporting this theory is looking at the elemental composition in the ITZs of the mixtures. If water from the LWA is encouraging pozzolanic reactions with PFA from the cement, it can be expected that PFA combines and consumes CH and forms new C–S–H gel, which is amorphous and accounts for the main strength of concrete [30]. Table 7 shows the variation in the Ca/Si ratio as a function of distance from the aggregate for both specimens. The quantitative analysis reveals for the gravel concrete specimen that a higher build-up of CH is mainly found in the interfacial zone. For the specimen with FAA, however, there is a fairly constant Ca/Si ratio and a relatively large quantity of C–S–H throughout the microstructure. Such a structure suggest that the microstructural development is much more uniform and extra C–S–H would eliminate the weak area at the ITZ somewhat, and more importantly the evidence points to the pozzolanic reaction occurring around the lightweight aggregate because of the high amounts of glassy phases present in the fly ash. A further way of supporting the theory is to measure CH content in the mortar of the samples. Fig. 7 shows combined DTA/TGA curves of the nixes in which the decomposition of CH occurs between 415° and 460°

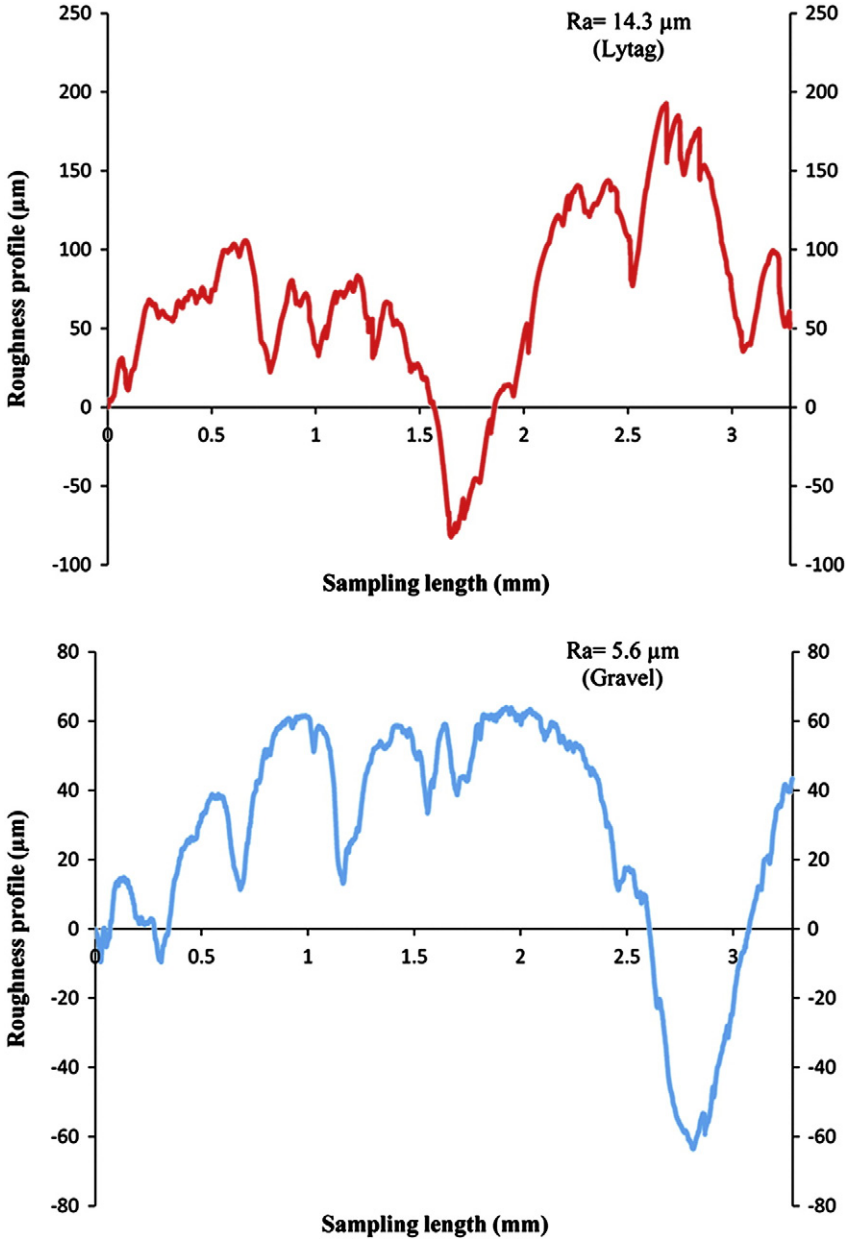

Fig. 5. Typical surface profiles of the aggregates used.

(conventional concrete), and 430° and 475° (lightweight concrete). The percentage weight loss corresponding to the dehydration of CH was measured as 1.70% for the lightweight mortar, while it was about 5.20% for the conventional concrete (the standard deviation of the analysis was 1.3 and 1.6% for the conventional and lightweight samples, respectively), indicating that pozzolanic reaction taking place in the lightweight mix reduces the CH content. At this point, it is believed that the w/c ratio used in this study may contribute to the development of pozzolanic reaction somewhat as the progress of cement hydration, which is a relatively fast process at a high w/c ratio, leads to moisture loss and thus releasing of the absorbed water from the pores of the material [31]. Thus, the high w/c may provide an active migration medium for movement of the mobile OH^- ions that attack to SiO_2 or Al_2O_3–SiO_2 framework for the primary pozzolanic reaction [32].

SEM micrographs for the paste surrounding the conventional and lightweight concrete are reproduced in Fig. 8(a) and (b), respectively. The porosity of the pastes deduced from the image analysis of the

Table 5
Geometrical parameters[a] of aggregates estimated by the Image Pro .

Aggregate	Area	Perimeter	Perimeter (convex)	Perimeter (ellipse)	Roundness	Angularity	Fractal dimension
Gravel	0.90	3.76	3.70	3.50	1.25	1.12	1.08
Sintered fly ash	0.99	1.12	3.55	3.53	1.01	1.00	1.02

[a] The units are in mm.

Table 6
Basic material properties at 28 days.

Concrete ID	Density (kg/m^3)	Compressive strength (MPa)	Flexural tensile strength (MPa)	Dynamic modulus of elasticity (GPa)
Conventional	2325	25.4	4.00	41.0
Lightweight	1895	28.7	3.15	23.7

Table 7
Ca/Si molar ratio at the ITZ.

Concrete	0 (μ)	10 (μ)	20 (μ)	30 (μ)	40 (μ)	50 (μ)
Conventional	2.20	0.82	2.62	2.70	3.22	2.84
Lightweight	0.46	1.90	2.00	2.59	2.26	2.40

micrographs as a function of the distance from the aggregate surface is also shown in Fig. 9. From the figure, it can be seen that the porosity of the paste surrounding the lightweight concrete at all distances was distinctively smaller than that of the paste around the conventional concrete. The error bars confirm the reliability of this comparison. Fig. 10 illustrates the close-up view of the ITZs in the conventional and lightweight concrete. It seems that a reduced amount of CH crystals and penetration of hydration products into surface pores of the aggregate (an example of EDX analysis is shown in Fig. 11) contributes to the development of a better bond and produce a relatively unfavorable place for crack formation in the ITZ, as also suggested by Wasserman and Bentur [33], and signifying that a higher local paste density has been achieved. Fig. 9 also shows that the thickness of the interfacial transition zone, where the porosity approaches to the level observed in the bulk paste, was approximately 15 μm and about 28 μm for the lightweight and conventional concrete, respectively. The reduction in the thickness of the ITZ may increase the integrity of the lightweight concrete by improving the contact point interactions for the matrix materials that flow and deform in the vicinity of the coarse aggregate, which in turn may enhance the concrete strength.

The most credible explanation of the strength of the FAA mixes, based on the results presented in this paper is that pozzolanic products, being the consequence of reaction of the fly ash in the cement with water released from the FAA and late hydration of previously unhydrated cement grains, are developing slowly after initial cement hydration process is complete. The water movements are almost certainly driven by developing matric and osmotic suctions in the paste during hydration. These products are helping to fill micro-pores in the paste in the ITZ. Due to the denser paste in the ITZ and rougher surface of the FAA, a stronger ITZ develops than would otherwise be the case and, certainly, stronger in the conventional concrete.

The flexural tensile strength of the FAA concrete was comparable and about 80% that of the conventional concrete. However, the increase in compressive cube strength with fly ash aggregate replacement is not replicated in flexure. This drop may be explained as follows: The flexural behavior could be dependent on both the surface roughness, which is leading factor for the interfacial bond strength, and the strength of the coarse aggregate. A deficiency or absence of one of these factors could result in flexural strength loss. Moreover, lightweight aggregate particles are much weaker than the surrounding matrix, and thus can be expected to crush more readily than do the gravel particles in the conventional concrete, leading to a less tortuous failure surface and a reduced contribution of

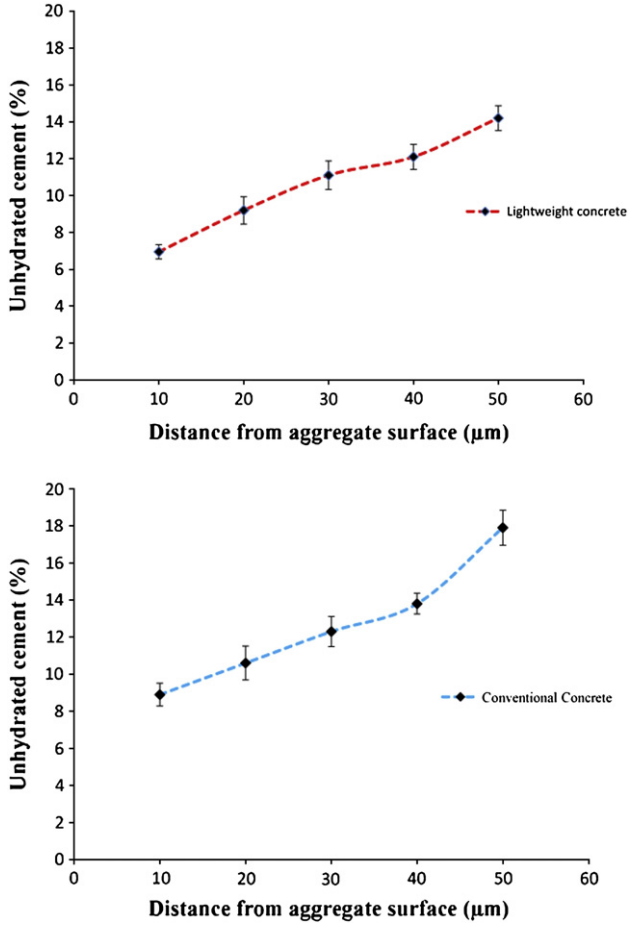

Fig. 6. Percent of unhydrated cement grains in the ITZs.

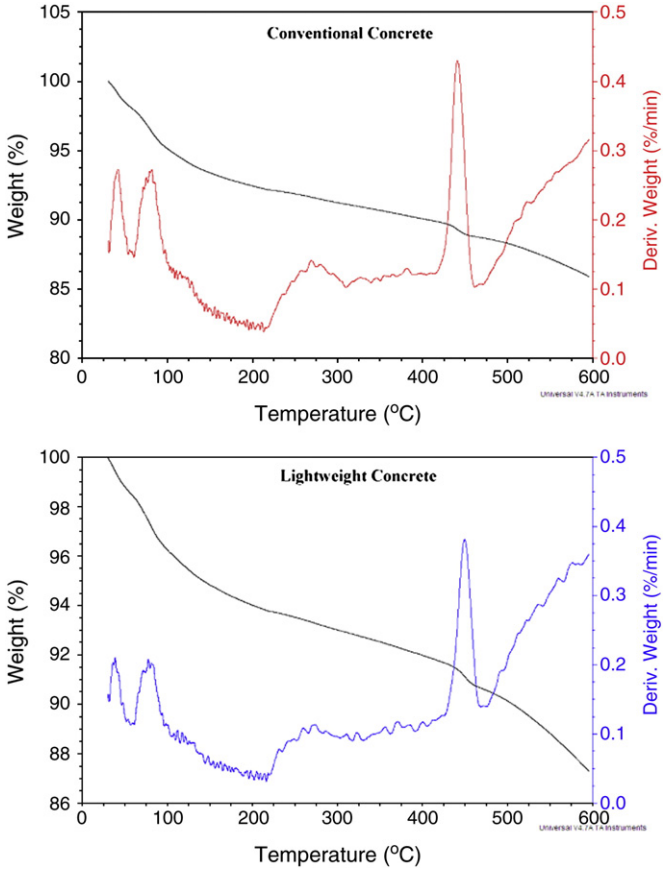

Fig. 7. DSC–TGA curves of the specimens.

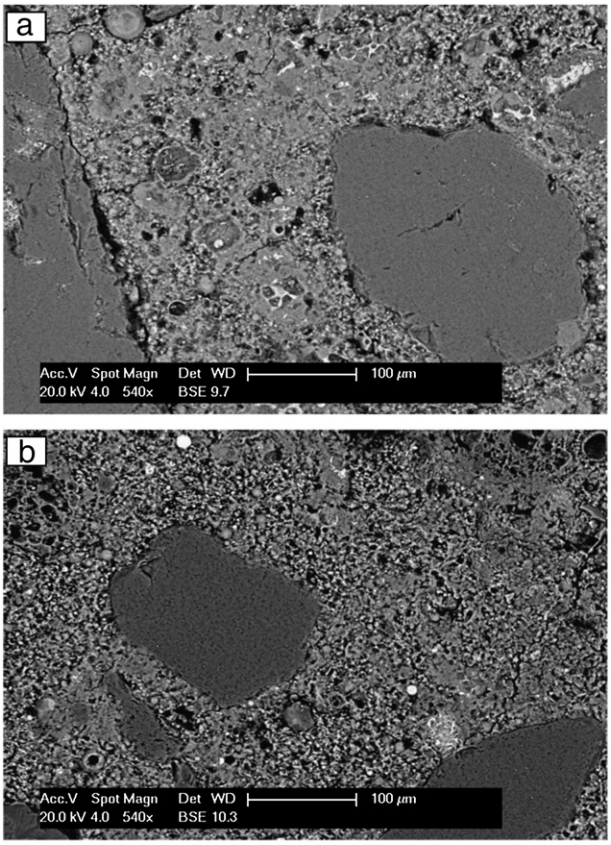

Fig. 8. SEM micrographs of the pastes surrounding the aggregates.

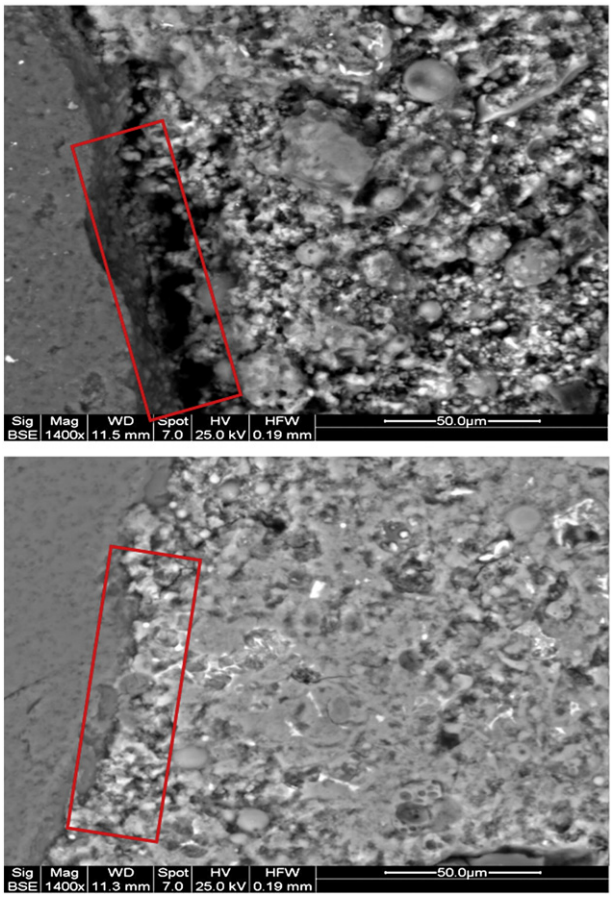

Fig. 10. Close up views of the ITZs.

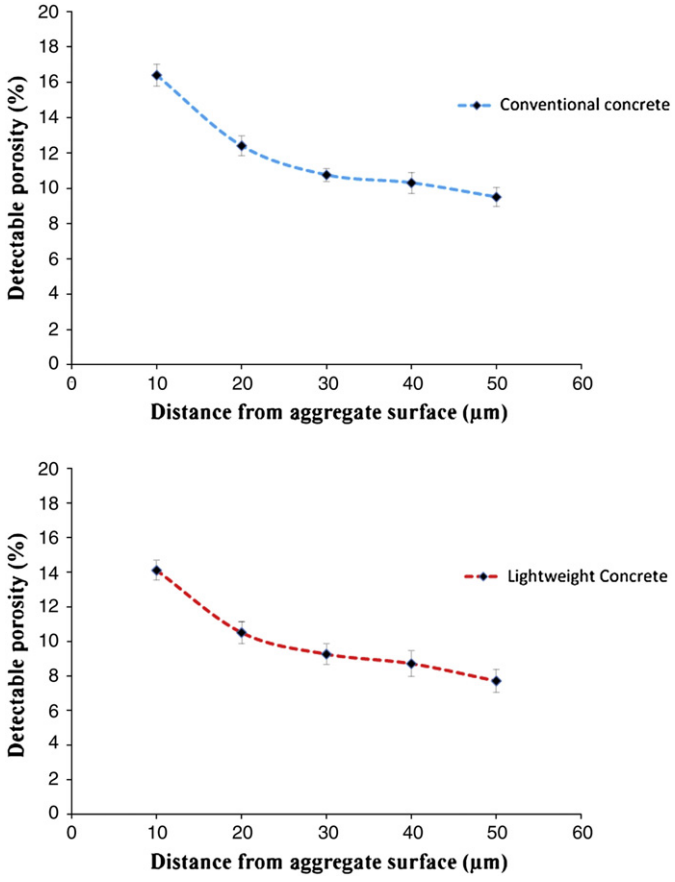

Fig. 9. Porosity profiles of the specimens at the interface.

aggregate interlock to the load transfer from the matrix to the aggregate with the generation of shear stresses under flexural loading. Thus, this mechanism would reduce the resistance of the FAA concrete to tensile strain, thus allowing it to fail at premature flexural strength level.

The concrete mixture prepared with FAA exhibited about 42% lower dynamic modulus of elasticity than concrete containing gravel aggregate, consistent with the findings by Tang et al. [25]. Given the denser packing (Fig. 9) of the FAA concrete, this is assumed to be because of the lower modulus of elasticity of the FAA compared to that gravel.

3.2.1. Flexural response accompanied by the microstructure

The loads versus average mid-span deflection responses for the conventional and lightweight concrete are depicted in Fig. 12.

As expected, after reaching peak load, neither concrete sample could carry any significant post-crack loads and collapsed within a very short time. It can be also seen from Table 8, that the first cracking and maximum load deflections for the conventional concrete are identical, while the first cracking and maximum load for the lightweight concrete are quite different (a much less linear pre-peak stress–strain curve). However, there were remarkable similarities in the post-peak region of the stress–strain curves. The conventional concrete started failing in an unstable manner. This behavior, from a fracture mechanics standpoint, might be attributable to the fact that the gravel particles were much stiffer than the surrounding cement matrix (i.e. a less homogeneous microstructure). Inhomogeneities cause strain incompatibilities within the mix and consequent localized stress concentrations and, hence, greater crack initiation and propagation points, eventually leading to accelerated failure accompanied by less energy dissipation within the lightweight specimen.

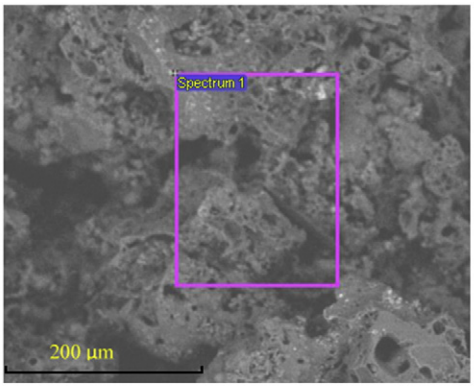

Element	Weight%	Atomic%	Compd%	Formula
C K	18.03	25.14	66.06	CO2
Na K	0.34	0.25	0.46	Na2O
Mg K	0.90	0.62	1.50	MgO
Si K	8.84	5.27	18.91	SiO2
P K	0.21	0.12	0.49	P2O5
S K	0.18	0.10	0.46	SO3
Cl K	0.06	0.03	0.00	
K K	0.99	0.43	1.20	K2O
Ca K	2.91	1.22	4.07	CaO
Ti K	0.30	0.11	0.50	TiO2
Fe K	4.73	1.42	6.09	FeO
Ni K	0.16	0.05	0.21	NiO
O	62.33	65.26		
Totals	100.00			

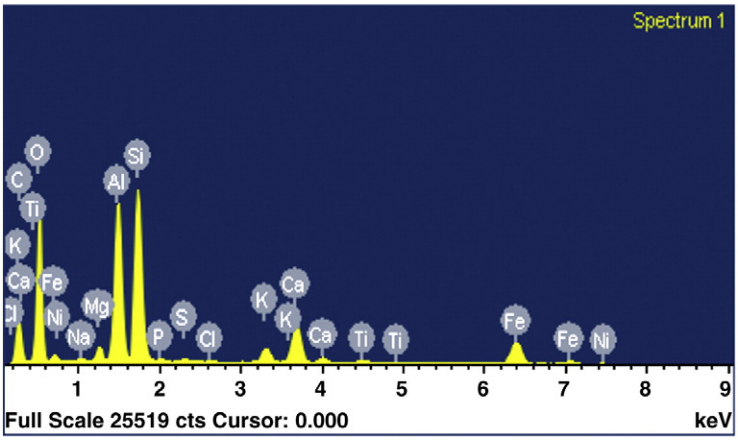

Fig. 11. Energy dispersive spectroscopy analysis in the pores of the FAA.

It is also worth highlighting that the deflection at the peak load for the FAA concrete is distinctively higher than that of the conventional concrete, although its peak load is much lower than that of the conventional concrete. This is basically an affect of mixture: a less stiff aggregate produced a less stiff concrete. A larger deflection is much more preferable under dynamic conditions such as impact or load fluctuations [34] due to the greater ability to absorb energy without yield. The high deflection value is also beneficial for fracture energy, which is the integral of the load vs. deflection curve, as seen in Table 8.

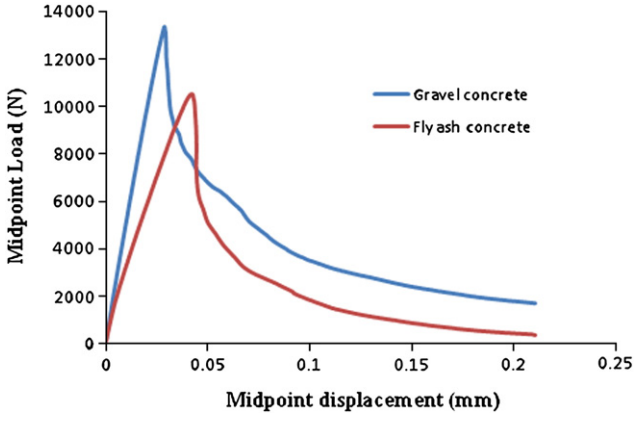

Fig. 12. Flexural load–displacement curves of the specimens.

3.3. Micro-structural damage investigation

Table 9 presents the impact strength results in terms of the number of blows to cause first crack and ultimate failure for both series of

Table 8
First crack loads, peak loads and corresponding deflections.

Concrete ID	First crack		Peak		Fracture energy[a]
	Deflection (mm)	Load (kN)	Deflection (mm)	Load (kN)	(kNm)
Conventional	0.028	13.36	0.028	13.36	1.51
Lightweight	0.0041	1.71	0.042	10.50	1.35

[a] Calculated from the area under load–deflection curve up to the point of failure.

Table 9
The results of drop-weight impact test.

Concrete ID	No. of blows for first crack			Average	No. of blows for ultimate failure			Average
	1	2	3		1	2	3	
Conventional	4	3	3	3	6	6	5	6
Lightweight	2	2	1	2	3	5	3	4

concrete mixtures. The data for three samples of each are recorded. As can be seen from Table 9, a relatively small number of blows were required to produce failure in the concrete specimens. They could endure only a few additional blows after the appearance of the first visible cracks.

Typical images captured to investigate micro-structural damage are presented in Figs. 13 and 14 for the lightweight concrete and conventional concrete, respectively. The concentrations of the micro-cracks in the ITZ could be an important parameter to help understand the failure process of the specimens subjected to impact loading. Table 10 shows the measured crack densities in the ITZ of the mixtures. As can be seen from Table 10, a much more concentrated damage occurred in the ITZ of the FAA (lightweight) concrete compared to that of the fly ash (lightweight) concrete. As highlighted by Akcaoglu et al. [35], the bigger the difference between the strengths of the ITZ and surrounding the matrix, the higher the tendency of micro-cracking in the ITZ. From this it may be inferred that the highly porous internal structure and rough internal texture of the FAA could possibly lead to a reduction in the grain–grain interlock and inter-particle friction within aggregate pieces, resulting in a less stiff material. By contrast, concrete made with gravel aggregates exhibited a different behavior; many interfaces between the matrix and the aggregate were debonded (as shown, e.g., in Fig. 15) most likely due to the weaker interface and the concrete had a much more tortuous fracture surface as a consequence.

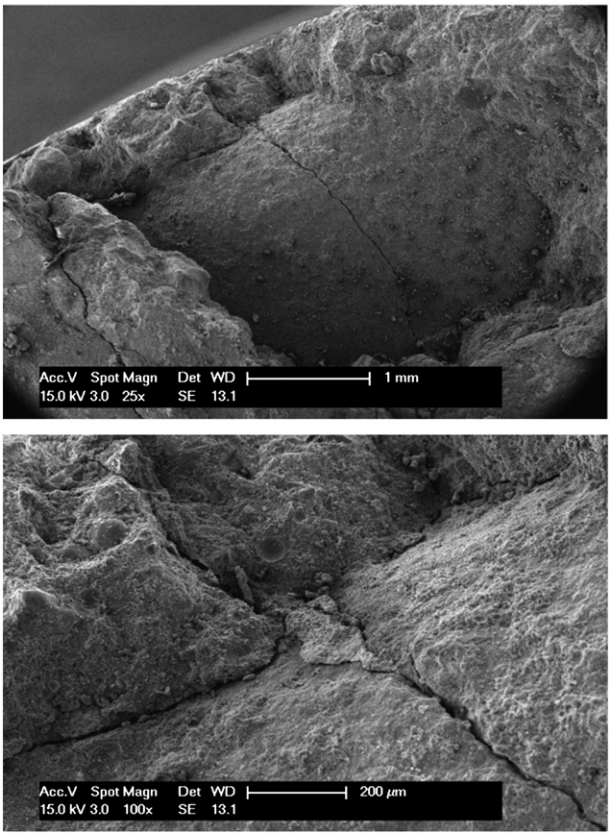

Fig. 13. Scanning electron micrographs for the lightweight concrete.

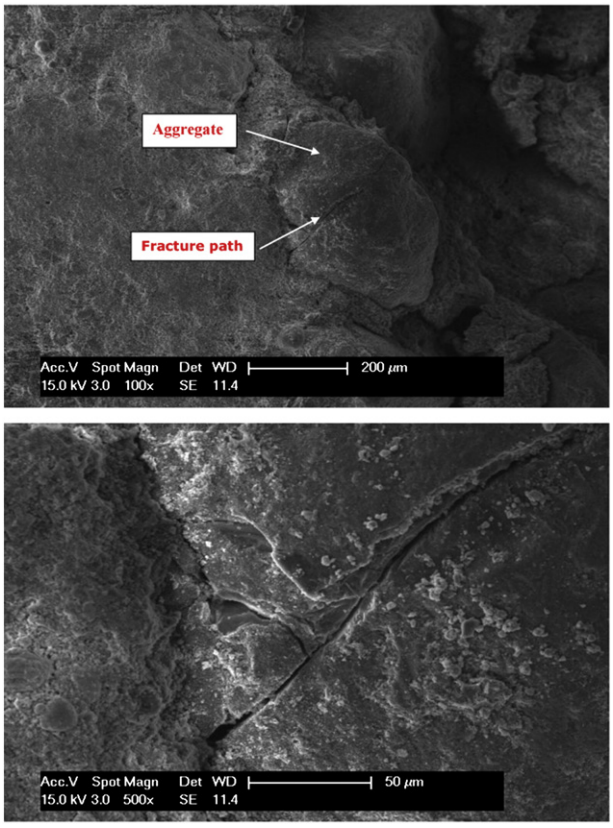

Fig. 14. Scanning electron micrographs for the conventional concrete.

As a contribution to the discussion of the failure mechanism involved in these concretes, a quantitative roughness analysis of the fracture surfaces was conducted to determine the microroughness number-Ra. The roughness profiles and calculated results of micro roughness are presented in Fig. 16 for the conventional and lightweight concrete, respectively. The results show that the microroughness of the conventional concrete is much larger than that of the lightweight concrete. There is already a theory that higher microroughness usually results in higher fracture energy consumption during the fracture and vice versa [36]. Figs. 17 and 18 show digitized crack maps of the surface, calculated fractal dimension of the cracks and fracture energies based on surface macro-crack measurement of the conventional and lightweight concrete specimens, respectively. The results give some support to the theory just mentioned and confirm that, for the concrete with gravel aggregates, greater fractal energies are dissipated during the impact event, mainly due to its more zigzag surface macro-crack pattern. When the lightweight concrete is subjected to the impact, relatively weak and less stiff the FAA cannot effectively spread the load, which in turn reduces the area need to

Table 10
Micro-crack density of the ITZ.

Concrete ID	Maximum crack width (μm)	Total crack length (μm)	Total crack area (μm^2)	Crack density (1/μm)
Conventional	28.90	705.9	9360.6	0.075
Lightweight	20.50	607.5	3627.55	0.167

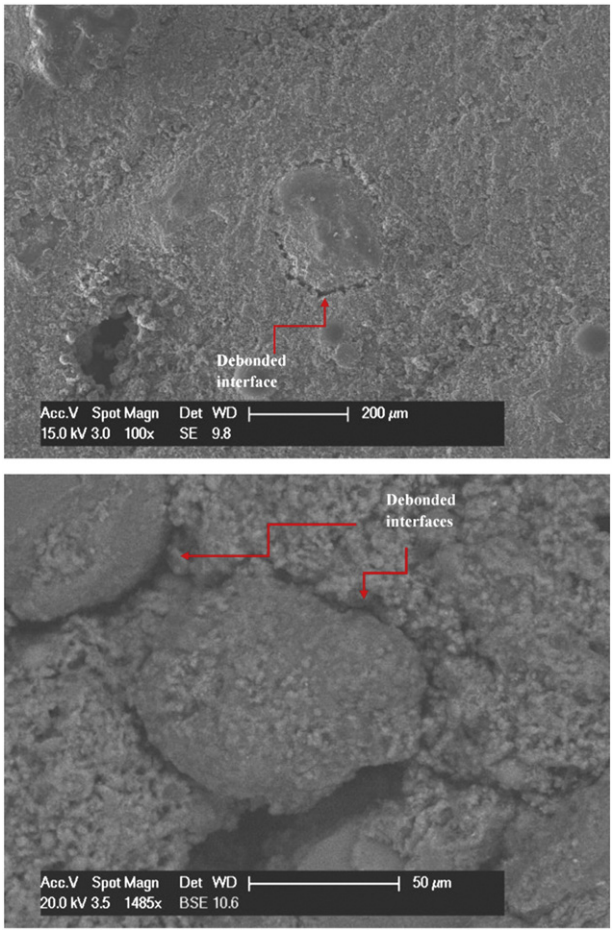

Fig. 15. Debonded interface in the conventional concrete.

be created on the surface during the fracture, and thus the concrete cannot resist to high level of plastic deformations and produces less tortuous fracture profile.

Fig. 19 compares the variation in relative dynamic modulus of elasticity of the conventional and lightweight concrete mixtures during impact exposure. The measurements have been performed in both horizontal and vertical (loading) directions just before and just after impact. It is obvious that the reduction in dynamic elastic modulus for the gravel concrete was more pronounced. This can be explained by the greater development of discontinuities at weak regions along the cement paste-aggregate bond and/or within the paste matrix of the gravel specimen due to impact-induced stress waves. In addition, it can also be assumed that the shock waves could interact with the secondary stress waves generated by structural inhomogeneities in the case of gravel specimen and further increase the anisotropic nature of concrete, leading to a sharp delay of velocity of travel time of the ultrasonic wave.

According to continuum damage mechanics, damage is caused as a result of nucleation, growth and coalescence of micro-voids. These voids may grow and generate new micro defects during the deformation process [37]. Thus, changes in air void distribution and content could also provide valuable information that can be linked to the damage process of concrete under impact. Fig. 20 presents the change in air void distribution across the depth of the conventional and lightweight specimens as a result of testing. As shown in Fig. 20, both specimens were heterogeneous with relatively low air voids concentrations in the bottom and top sections, and a relatively higher air void concentrations in the middle part of the specimens (much more pronounced in the lightweight concrete specimen), signifying that the damage is a localized phenomenon occurring in a critical location in a heterogeneous material in accordance with the findings of Ying [21].

The level of damage taking place during the impact testing was quantified through the damage parameter ξ, previously described in Section 2.3.3. Fig. 21 presents the calculated damage parameters for

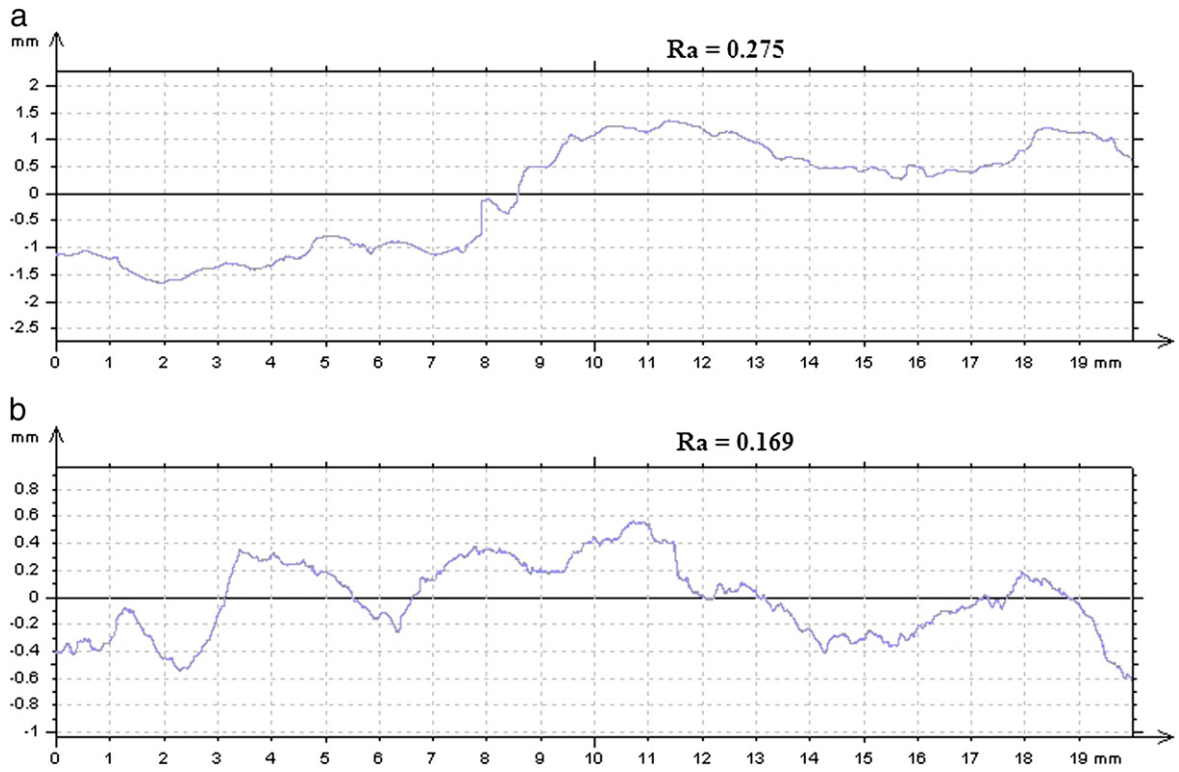

Fig. 16. Micro roughness profiles of the lightweight concrete (a) the conventional concrete (b) after impact.

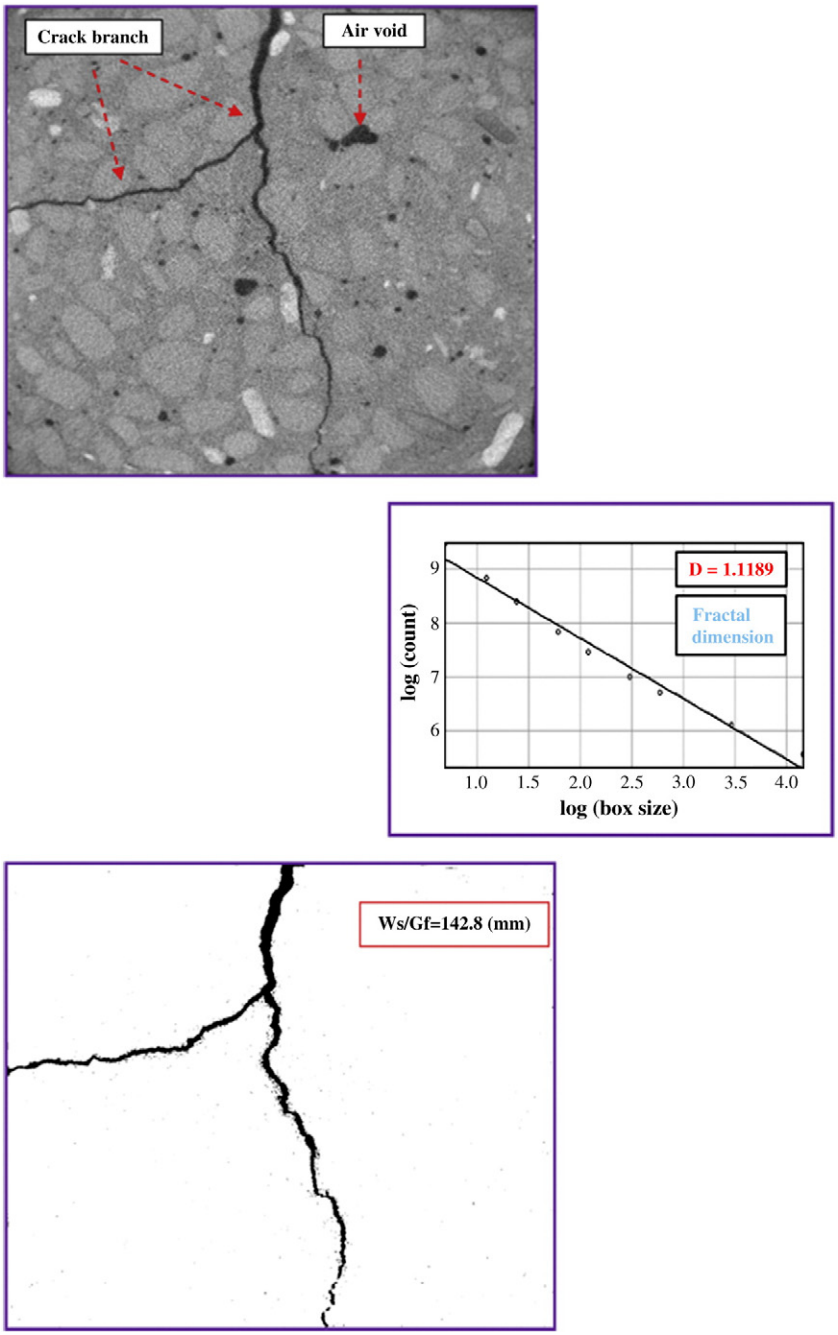

Fig. 17. Digitized crack maps and fractal energy of the conventional specimen.

the conventional and lightweight specimens, respectively. These results suggest that most of the damage taking place in the middle part of the lightweight specimens compared to its top and bottom sections, which likely contributes to a brittle fracture process associated with low energy dissipation under impact loading. Because less energy dissipation associated with an inhomogeneous microstructure would reduce the propagation of reflected tension waves from the rear surface of concrete and correspondingly generate a non-uniform stress distribution and high level localized plastic deformations. By contrast, the conventional specimen had a relatively higher damage in top part while the middle and bottom sections were damaged almost equally.

Based on the visual observation carried out on the cracking faces, it was observed that the failure for the conventional concrete was created by the destruction of the aggregate-paste interface or the paste, whereas almost all lightweight aggregates were fractured across their diameters. Of course, such results are predictable or already well-known (i.e. failure through lightweight aggregate or gravel pull-out under impact). The merit of this research is to provide a quantitative microstructural analysis from which it may be possible, in the future, to establish a numerical model for the fracture process or to correlate the microstructure of concrete with its mechanical properties.

4. Concluding remarks

In the light of the findings obtained from this experimental study, the following conclusions can be drawn:

- Concrete with pre-wetted lightweight ash aggregates had a higher cube compressive strength than the conventional concrete with

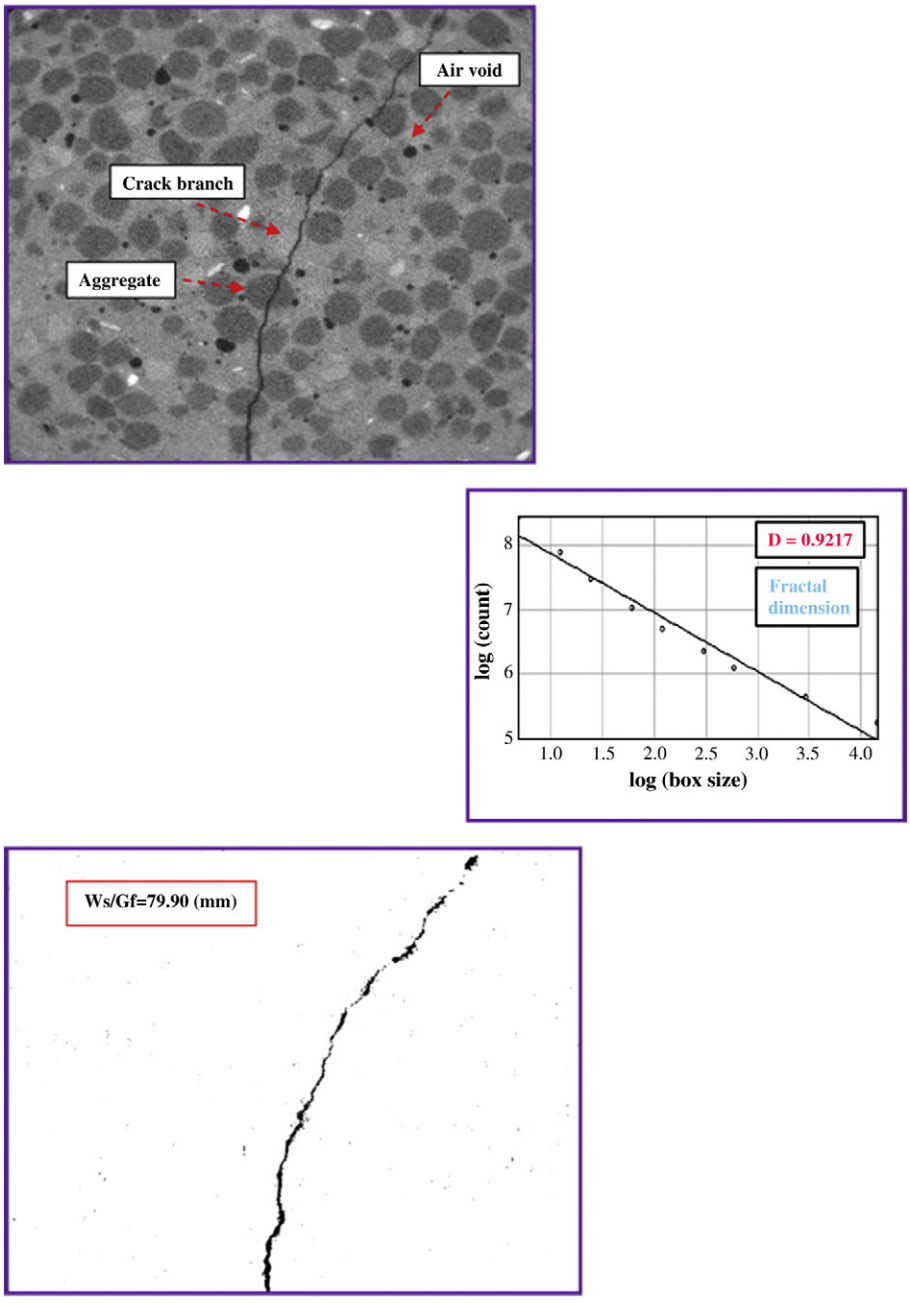

Fig. 18. Digitized crack maps and fractal energy of the lightweight specimen.

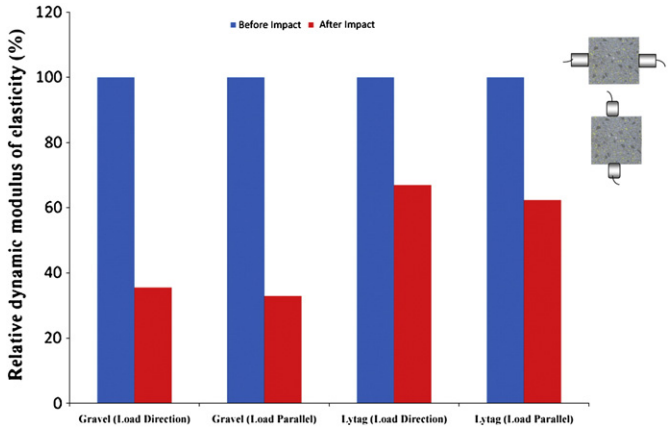

Fig. 19. The variation in dynamic modulus of elasticity of the mixes.

gravel. The higher compressive strength of the FAA concrete compared with that of the conventional concrete is likely due to enhanced hydration as a result of internal curing (confirmed from the characterization of interfacial porosity and the thermogravimetric analysis). However, the flexural tensile strength and the dynamic modulus of elasticity of the lightweight concrete are respectively about 20% and 44% lower than the corresponding values of the conventional concrete.

- A micro-structural study revealed that a relatively dense and homogeneous interface with a moderate amount of C–S–H gels was present between the FAA and cement matrix in the lightweight concrete, while a more porous and loose interface existed in the conventional concrete due to the presence of calcium hydroxide crystals and internal voids that could, presumably, provide a line of weakness for failure to take place along, and thus lead to less strength.
- As observed for the impact behavior, the FAA concrete seems to be more brittle than the gravel aggregate concrete. It is believed that the less homogeneous micro-structure of the lightweight concrete

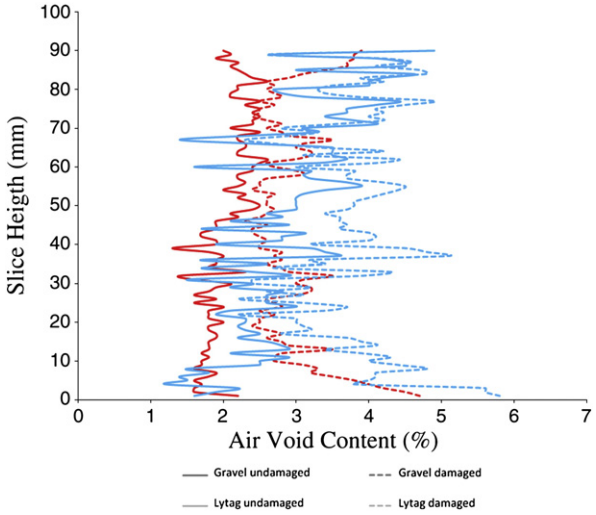

Fig. 20. The changes in air void distribution across the depth of the mixes.

would lead to strain incompatibilities and consequent localized stress concentrations and, hence, greater crack initiation and growth points, leading to accelerated failure accompanied by less energy dissipation.

- Under impact loading, failure of concrete containing gravel aggregates occurred through the ITZ; mainly including pull-out of individual aggregate pieces from their cavities. Concrete prepared with the FAA failed through the aggregates; primarily including splitting of the aggregates across their diameter. Analysis for the real fracture profiles with a non-contact laser profilometer showed that the physical and microstructural aspects of aggregate may lead to a reduction in microroughness and correspondingly the amount of fracture energy.

Acknowledgments

The authors would like to gratefully acknowledge Dr. M.T. Bassuoni (University of Nottingham) for the input of helpful discussion and advice. Special thanks must also go to research students Mr. Peter Bayliss and Ms. Lindy Heath (School of Chemistry—University of Nottingham) for their valuable helps and comments during the XRD and TGA analyses. The authors wish also to thank Alan Beattie, who is Technical& Quality manager of Lytag Ltd., for his interest in this work and for providing the sintered fly ash aggregates.

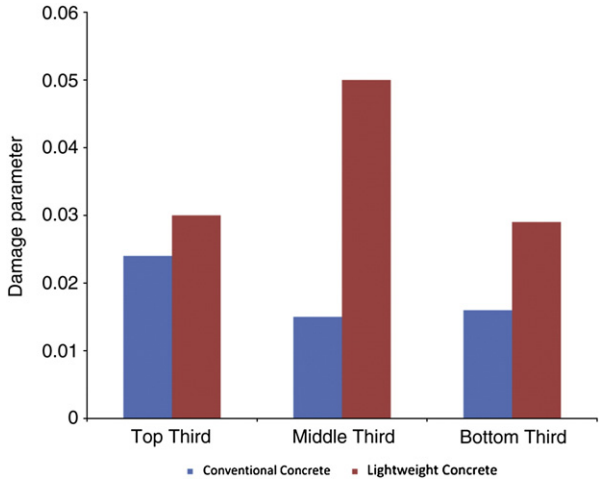

Fig. 21. Calculated damage parameters ξ in the top, middle and bottom third sections.

References

[1] H.S. Wong, M. Zobel, N.R. Buenfeld, R.W. Zimmerman, Influence of the interfacial transition zone and micro-cracking on the diffusivity, permeability and sorptivity of cement based materials after drying, Mag. Concr. Res. 61 (2009) 571–589.
[2] A. Bentur, M.G. Alexander, D. Bentz, O. Buyukozturk, J. Elsen, D. Hooton, H. Jennings, A. Katzs, K.O. Kjellsen, A. Kronlof, B. Laggerblad, S. Mindess, J.P. Ollivier, K. Scrivener, J. Skalny, et al., Review of the work of the RILEM TC 159-ETC: engineering of the interfacial transition zone in cementitious composites, Mater. Struct. 33 (2000) 82–87.
[3] J.J. Zheng, C.Q. Li, X.Z. Zhou, Thickness of interfacial transition zone and cement paste content profiles around aggregates, Mag. Concr. Res. 57 (2005) 397–406.
[4] A. Cwirzen, V. Penttala, Aggregate-cement paste transition zone properties affecting the salt-frost damage of high-performance concrete, Cem. Concr. Res. 35 (2005) 671–679.
[5] P. Soroushian, M. Elzafraney, Damage effects on concrete performance and microstructure, Cem. Concr. Compos. 26 (2004) 853–859.
[6] D.P. Bentz, Influence of internal curing using lightweight aggregates on interfacial transition zone percolation and chloride ingress in mortars, Cem. Concr. Compos. 31 (2009) 285–289.
[7] M.H. Zhang, O.E. Gjørv, Pozzolanic reactivity of lightweight aggregates, Cem. Concr. Res. 20 (1990) 884–890.
[8] S. Weber, H.W. Reinhardt, A new generation of high performance concrete: concrete with autogenous curing, Adv. Cem. Based Mater. 6 (1997) 59–68.
[9] O. Kayali, Fly ash lightweight aggregates in high performance concrete, Constr. Build. Mater. 22 (2008) 2393–2399.
[10] T. Krauthammer, M.M. Elfahal, J. Lim, T. Ohno, M. Beppu, G. Markeset, Size effect for high-strength concrete cylinders subjected to axial impact, Int. J. Impact Eng. 28 (2003) 1001–1016.
[11] T. Tang, H. Saadatmanesh, Behaviour of concrete beams strengthened with fiber-reinforced polymer laminates under impact loading, J. Compos. Constr. 7 (2003) 209–218.
[12] M. Nili, V. Afroughsabet, Combined effect of silica fume and steel fibers on the impact resistance and mechanical properties of concrete, Int. J. Impact Eng. 37 (2010) 879–886.
[13] P. Sukontasukkul, P. Nimityongskul, S. Mindess, Effect of loading rate on damage of concrete, Cem. Concr. Res. 34 (2004) 2127–2134.
[14] N. Wang, S. Mindess, K. Ko, Fibre reinforced concrete beams under impact loading, Cem. Concr. Res. 26 (1996) 363–376.
[15] S. Mindess, C. Yan, Perforation of plain and fibre reinforced concretes subjected to low velocity impact loading, Cem. Concr. Res. 23 (1993) 83–92.
[16] N. Banthia, C. Yan, K. Sakai, Impact resistance of fiber reinforced concrete at subnormal temperatures, Cem. Concr. Compos. 20 (1998) 393–404.
[17] BS EN 197–1:2000, Cement Part 1: Composition, Specifications and Conformity Criteria for Common Cements, British Standard Institution, London, 2000.
[18] BS EN 13139: 2002, Aggregates for Mortar, British Standard Institution, London, 2002.
[19] J. Müller-Rochholz, Determination of the elastic properties of lightweight aggregate by ultrasonic pulse velocity measurements, Int. J. Cem. Compos. Lightweight Concr. 1 (1979) 87–90.
[20] ACI Committee 544, Measurement of properties of fiber reinforced concrete, ACI Mater. J. 85 (1988) 583–593.
[21] H. Ying, X-ray computed tomography to quantify damage of hot-mix asphalt in the dynamic complex modulus and flow number tests, MSc thesis, Louisiane State University, 2010.
[22] L.P. Guo, W. Sun, K.R. Zheng, H.J. Chen, B. Liu, Study on the flexural fatigue performance and fractal mechanism of concrete with high proportions of ground granulated blast-furnace slag, Cem. Concr. Res. 37 (2007) 242–250.
[23] K.L. Scrivener, P.L. Pratt, A preliminary study of the microstructure of the cement/sand bond in mortars, Proceedings of 8th International Congress of the Chemistry of Cement, Rio de Janerio, 1986, pp. 466–471.
[24] S.F. Lee, S. Jacobsen, Study of interfacial microstructure, fracture energy, compressive energy and debonding load of steel fiber-reinforced mortar, Mater. Struct. (2011), doi:10.1617/s11527-011-9710-4.
[25] W.C. Tang, T.Y. Lo, W.K. Chan, Fracture properties of normal and lightweight high-strength concrete, Mag. Concr. Res. 60 (2008) 237–244.
[26] R.V. Balendran, F.P. Zhou, A. Nadeem, A.Y.T. Leung, Influence of steel fibres on strength and ductility of normal and lightweight high strength concrete, Build. Environ. 37 (2002) 1361–1367.
[27] F.P. Zhou, F.D. Lydon, B.I.G. Barr, Effect of coarse aggregate on elastic modulus and compressive strength of high performance concrete, Cem. Concr. Res. 25 (1995) 177–186.
[28] G.E. Hijazin, M. Lopez, Extending internal curing to concrete mixtures with w/c higher than 0.42, Constr. Build. Mater. 25 (2011) 1236–1242.
[29] D.P. Bentz, Internal curing of high performance blended cement mortars, ACI Mater. J. 104 (2007) 408–414.
[30] S. Chatterji, Concrete durability and CaO/SiO mole ratio of CSH, Cem. Concr. Res. 25 (1995) 929–932.
[31] N.V. Tuan, G. Ye, K.V. Breugel, O. Copuroglu, Hydration and microstructure of ultra high performance concrete incorporating rice husk ash, Cem. Concr. Res. (2011), doi:10.1016/j.cemconres.2011.06.009.
[32] H.F.W. Taylor, Cement Chemistry, 2nd edition Thomas Telford Publishing, London, 1997.

[33] R. Wasserman, A. Bentur, Interfacial interactions in lightweight aggregate concretes and their influence on the concrete strength, Cem. Concr. Compos. 18 (1996) 67–76.
[34] J. Newman, P. Owens, Properties of lightweight concrete, in: J. Newman, B.S. Choo (Eds.), Advanced Concrete Technology, Processes, Butterworth- Heinemann, Great Britain, 2003.
[35] T. Akçaoğlu, M. Tokyay, T. Çelik, Assessing the ITZ micro-cracking via scanning electron microscope and its effect o the failure behaviour of concrete, Cem. Concr. Res. 35 (2005) 358–363.
[36] K. Wu, A. Yan, W. Yao, D. Zhang, Effect of metallic aggregate on strength and fracture properties of HPC, Cem. Concr. Res. 31 (2001) 113–118.
[37] R. Khan, Quantification of micro-structural damage in asphalt, PhD thesis, University of Nottingham, United Kingdom, 2009.